The Influence of Prior Microstructure on Tempering Stages in 2.25Cr-1Mo Steel

P.Parameswaran, M.Vijayalakshmi and V.S.Raghunathan

Materials Characterisation Group, Indira Gandhi Centre for Atomic Research, Kalpakkam-603 102, India

(Received October 28, 2002.)

ABSTRACT

The influence of prior microstructure on the tempering behaviour of 2.25Cr-1Mo steel at two different temperatures is reported in this paper. The tempering behaviour of the steel could be classified into four different stages. The prior microstructure, namely the amount of bainite, was found to influence the following three characteristics: 1) the extent of secondary hardening, 2) time to reach peak hardness and 3) the saturation level of hardness. The observed influence of prior microstructure on tempering behaviour has been understood in terms of the synergistic effect of a number of microstructural changes, like the modification of bainite, growth of a number of carbides and the recovery processes. The paper discusses the influence of two different prior microstructures on the above features of tempering behaviour, at two temperatures.

1. INTRODUCTION

The modification of properties, specifically mechanical properties, during exposure to elevated temperature is of important concern for materials used in high temperature applications such as steam generators in power plants. The steam generators of nuclear power plants use 2.25 Cr -1 Mo steel in the evaporator circuits for their tubings /1/. The initial microstructure of this material undergoes morphological and microchemical changes as a consequence of exposure to high temperatures during service. The steel is supplied in the normalised and tempered condition (austenitized at 1323K/1h and tempered at 1023K/1h) for commercial applications /2/. In this condition, the initial microstructure of the steel consists of ferrite with carbides. However, this microstructure is not in stable equilibrium and it continues to evolve slowly during the high temperature applications /3,4/. The exposure to elevated temperature would result in microstructural evolution in the form of recrystallisation, grain coarsening and nucleation and growth of secondary carbides. Additionally, decarburisation due to mass transfer between the structural materials of the steam generators and the intermediate heat exchangers in liquid metal fast breeder reactors has indicated that loss of carbon would modify the microstructure and hence the mechanical properties /5/. These microstructural modifications in the steel are likely to affect its creep properties. Microstructural changes in the steel during prolonged exposure sometimes lead to deterioration of ductility and strength /6/. Precipitation behaviour, dislocation and substructure rearrangement would affect the mechanical properties of ferritic steels significantly /7/. Hence, study of the microstructural evolution has attracted the attention of many researchers /8, 9/.

It is observed that a good combination of mechanical properties is achieved by the judicious choice of the initial microstructure /10/, with a higher degree of stability during the life time (~ 30 years) of the components. Further different initial microstructures are

likely when these structures are produced through thermomechanical processing. Hence in this paper, a systematic study is carried out to understand the nature of microstructural evolution that occurs when a 2.25 Cr-1Mo steel with two different prior microstructural conditions is exposed to elevated temperatures.

2.EXPERIMENTAL

The material used was 2.25 Cr - 1Mo steel supplied by M/s Creusot Loire, France. The composition of the steel evaluated by bulk chemical compositional analysis is shown in Table I.

Table I

Nominal composition of the steel used (in wt %)

C	Si	Mn	P	Mo	Cr	Fe
0.11	0.31	0.4	0.025	0.9	2.25	Bal.

Samples of 10 mm diameter and 20 mm thickness were austenitized at 1323K for 1h and were cooled in 1) air and 2) flowing argon gas respectively. Thermocouples were attached to the samples and temperatures were measured as the samples cooled to room temperature through the different cooling media. The cooling rate achieved through air cooling was found to be ~1K/s, while in Ar it was found to be approximately 0.1K/s. The specimens exposed to two different cooling rates (1K/s and 0.1K/s) will be referred to hereafter as steel A and steel B respectively. The samples were further aged at 923 and 1023K for durations ranging from 2 to 50h. The tempering behaviour was studied by the measurements of macro hardness values of the samples as a function of the time of exposure at high temperature using Vickers macrohardness tester, using a load of 1Kg.

Optical microscopy was carried out to characterise the initial microstructures after careful metallographic preparation of the samples. The percentage of bainite was measured from the optical micrographs by conventional quantitative metallographic techniques and expressed as the ratio of area of bainite to total area /11/.

Samples for electron microscopy were prepared by electropolishing thin slices in an electrolyte mixture of 10% perchloric acid and 90% acetic acid. Carbon extraction replica technique was used to prepare replica from the well-etched samples. The thin foils and the carbon extraction replicas were examined using Analytical Transmission Electron Microscope (Philips EM400T attached with Link Energy dispersive X ray analyser).

3. RESULTS AND DISCUSSION

3. 1.Characterisation of initial microstructure

The steel when cooled in air (1K/s) after the initial austenitization treatment exhibited a fully bainitic structure (Steel A). Fig. 1(a) shows the optical micrograph exemplifying the typical fully bainitic structure exhibited by this steel. The cooling rate was high enough for high temperature austenite to bypass the ferrite start nose temperature, 1000K, and transform completely into bainite.

On the other hand, 2.25Cr-1Mo steel when cooled in argon after austenitizing at 1323K resulted in a mixture of ferrite and bainite, simply referred hereafter as ferrito-bainite (steel B). The cooling rate being slower (0.1K/s), the formation of proeutectoid ferrite at high temperature could not be suppressed and the remaining austenite transformed to bainite, when Bs temperature, 833K was reached. The microstructure shown in Fig. 1(b) is a typical ferrito-bainitic structure observed in this steel. The area fraction of bainite was measured from optical micrographs /11/, and was found to be 30% in steel B.

Fig. 1(c) shows the TTT curve of 2.25 Cr-1 Mo steel available in the literature /1/. The cooling rates for the two steels are superimposed on the TTT diagram. It can be inferred that the steel A on cooling from austenitizing temperature bypasses the ferrite start nose temperature, but passes through the bainitic region. Hence it is clear that the steel A has completely transformed into bainite, while on the other hand, steel B cools quite slowly and comparatively by one order less. The transformation of austenite to ferrite at the temperature range 1050K to 923K is therefore unavoidable, much before the temperature for the bainitic transformation temperature, B_s (= 833K), is reached. Hence the microstructure that ensued was

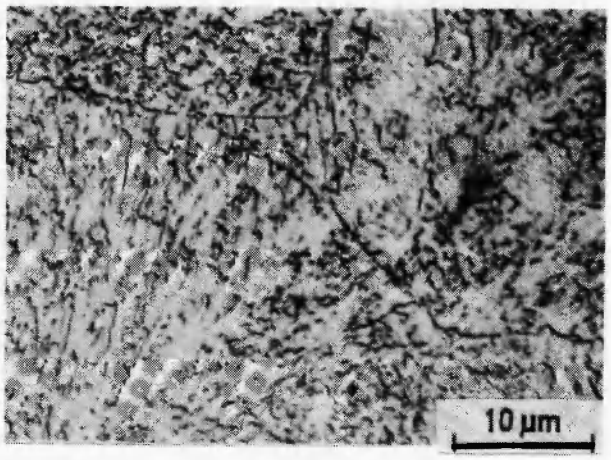

Fig. 1(a): Optical micrograph showing the fully bainitic structure present in steel A.

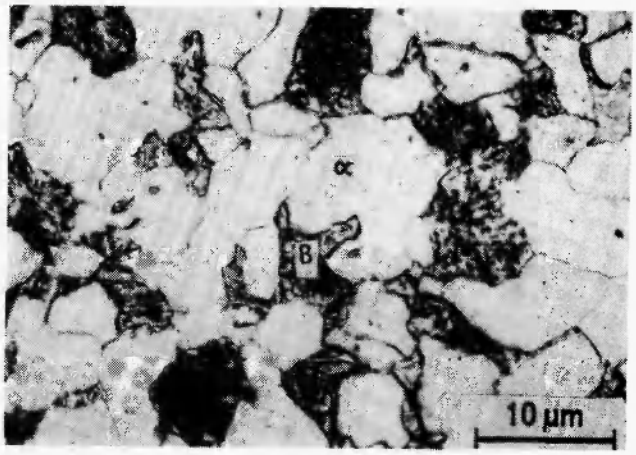

Fig. 1(b): Optical micrograph showing ferrite-bainitic structure in steel B. The regions ferrite and bainite are marked as α and B in the figure.

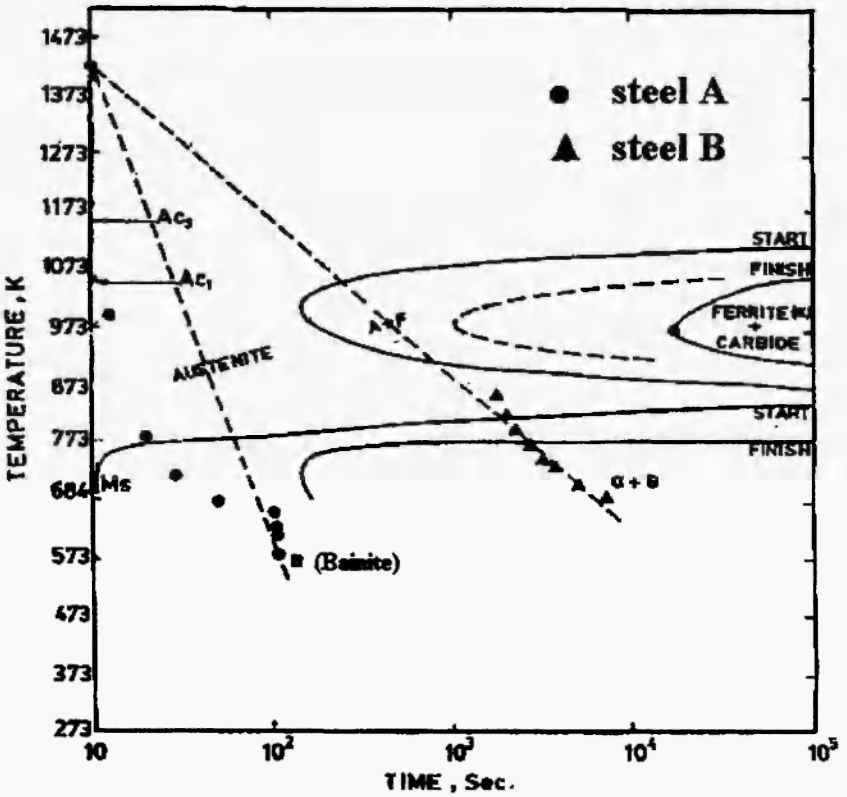

Fig. 1(c): The different cooling rates superimposed on the TTT diagram [Ref.1] of 2.25Cr-1Mo-0.1C steel. Steel A refers to air cooling and Steel B refers to furnace cooling with Ar purging.

ferrito-bainitic.

To understand the nature of the bainite, transmission electron microscopy of the two steels was carried out. It is observed from the transmission electron micrographs that the nature of bainite in the two steels was not similar and is different. (Fig. 2 (a) and (b)). While steel A (Fig.2(a)) shows complete bainitic microstructure, the steel B (Fig.2(b)) shows proeutectoid ferrite free of carbides and bainite which is distinctly granular. The carbides inside the bainite grains, for example, in Fig. 2b were analysed using Selected Area Diffraction (SAD) patterns and a representative pattern is shown in Fig. 2(c) along with its key (Fig.2.(d)). The analysis indicates the zone axis of the carbide as [$\bar{1}11$] of M_3C type carbide. Fig. 2(e) shows the EDX spectrum of one of the carbides which is found to be Fe-rich, in consistency with the SAD analysis, suggesting the formation of Fe-rich Fe_3C type of carbides.

Fig. 2(a): Transmission electron micrograph of the initial microstructure of steel A showing laths of bainite.

Fig. 2(b): Transmission electron micrograph of the initial microstructure of steel B showing granular bainite along with proeutectoid ferrite

Fig. 2(c): SAD pattern from one of the carbides present in bainite of Fig.2b.

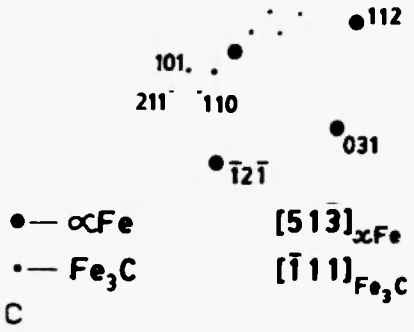

Fig. 2(d): Key for identification of the carbide, M_3C.

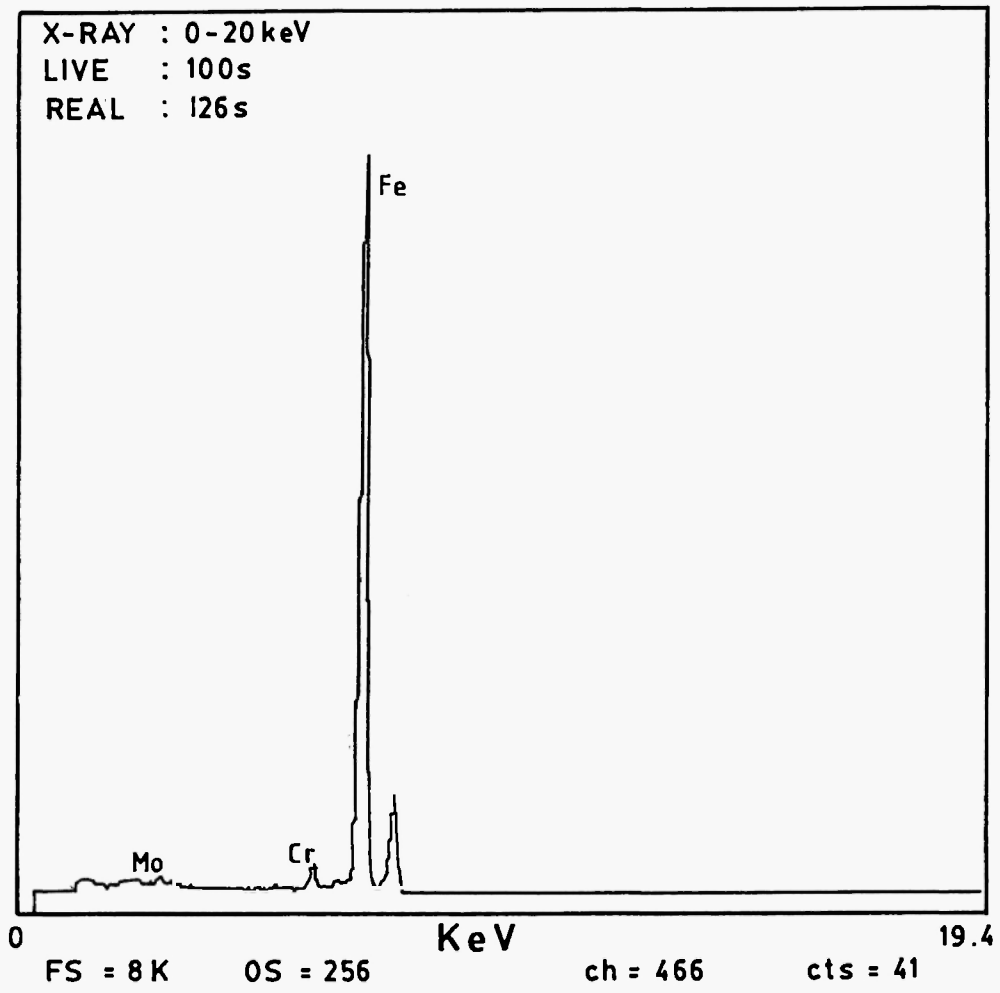

Fig. 2(e): EDX spectrum from one of the carbides present in steel B shown in fig.2b.

3.2. Effect of prior microstructure on tempering behaviour

Having observed that the initial microstructures of the steels are quite distinct, the high temperature tempering behaviour is also expected to be different. Fig. 3 shows the variation of macrohardness of the two steels with time of exposure at two different temperatures. It is apparent from Fig. 3 that steel A exhibits higher initial hardness than steel B. While steel A exhibited an initial macrohardness value of 340 VHN, steel B showed 165 VHN only. This is due to the complete transformation of austenite into 100% bainite in steel A in contrast to the formation of 70% soft pro-eutectoid ferrite in Steel B.

Exposure of these steels at 923 and 1023K leads to simultaneous modification of bainite and transformation of primary cementite particles to a series of secondary carbides, M_2C, M_7C_3, $M_{23}C_6$, M_6C etc. /12/. The carbide stability diagram /13/ is a modified diagram of that proposed in reference /12/ incorporating the consideration that different types of metal atoms share the unit cell in these carbides (for example, Cr_7C_3 is referred to here as M_7C_3 to indicate that other atoms are likely to be incorporated in the carbide structure). The sequence of carbide precipitation observed in the present study is in general agreement with that reported in reference /12/. The sequence of the carbide precipitation of Steel A on tempering can be

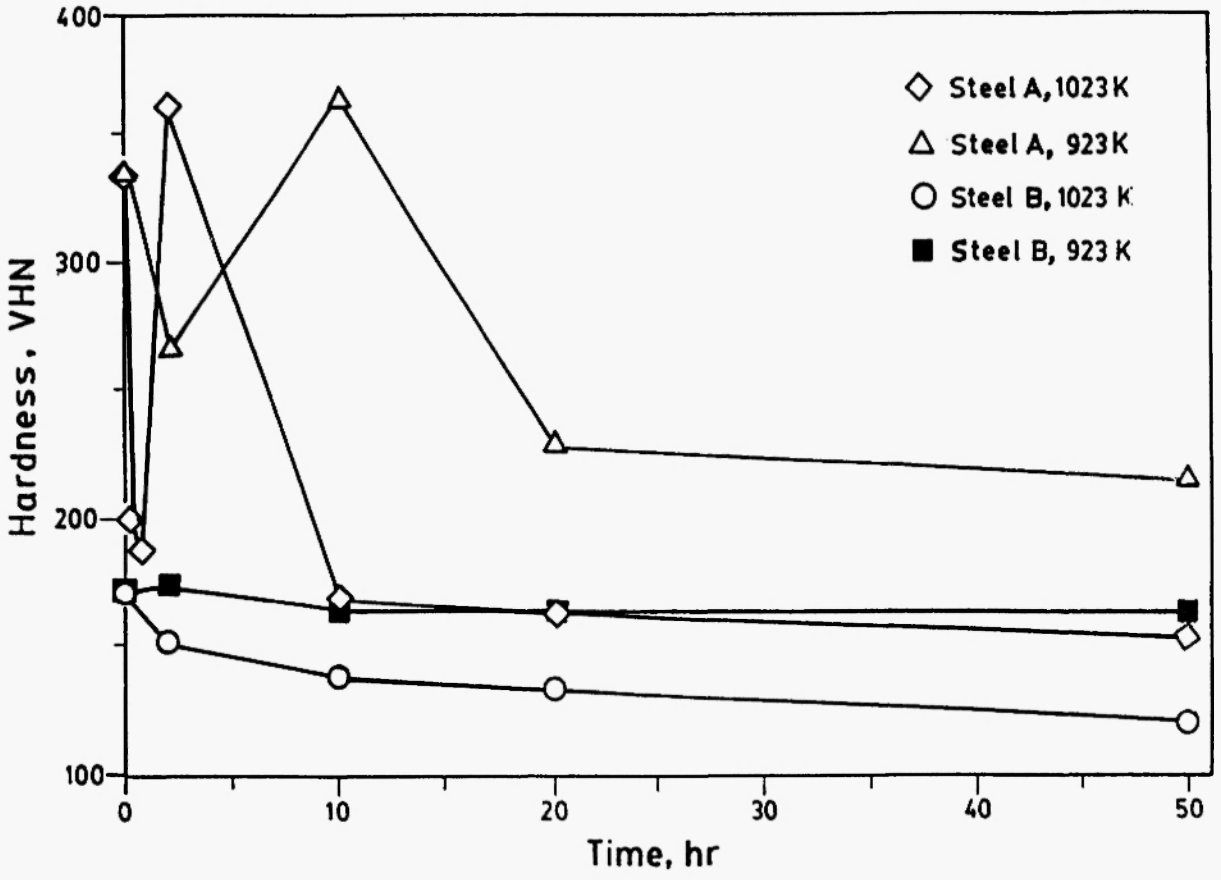

Fig. 3: Variation of macrohardness as a function of tempering time for the two different steels.

summarised as follows:

Bainite $(\alpha+M_3C)\rightarrow(\alpha+M_2C) \rightarrow (\alpha+M_7C_3)\rightarrow(\alpha + M_{23}C_6+M_6C)$

This sequence can be compared with the sequence given in ref. /13/:

Bainite $\rightarrow (\alpha+M_2C) \rightarrow(\alpha+M_{23}C_6)$

$\downarrow \quad \rightarrow \alpha+M_6C$

$\rightarrow \alpha+M_7C_3$

The sequence observed in steel B can be summarised as:

Bainite $(\alpha + M_3C) \rightarrow (\alpha +M_2C) \rightarrow (\alpha+M_7C_3)\rightarrow(\alpha + M_{23}C_6)$

Proeutectoid $\alpha\rightarrow(\alpha+M_2C)\rightarrow (\alpha +M_{23}C_6)$

The above sequence nearly follows the sequence presented by Baker and Nutting /12/, namely:

Bainite $(\alpha + F_3C) \rightarrow \alpha + Mo_2C \rightarrow \alpha + M_7C_3\rightarrow\alpha+M_{23}C_6\rightarrow\alpha+M_6C$

Ferrite,$\alpha\rightarrow \alpha+Mo_2C\rightarrow \alpha+M_6C$

On comparing the sequence of evolution of carbides in the present study with the available literature, a major difference pertains to the equilibrium structure of $(\alpha+M_6C)$ in Ref. /12/ in contrast to $(\alpha +M_{23}C_6)$ in the present study. This can be related to the longer tempering times of 1000h employed in earlier work compared to a shorter time of 50h in the present study. The formation of M_6C occurs only for times higher than 100h for tempering at temperatures above 973K due to slower kinetics prevailing in this temperature.

The exact sequence and microchemical nature of these carbides are discussed in detail elsewhere /14,15/.

The most relevant information in the context of the present study is that the carbides that promote softening were identified as M_7C_3, $M_{23}C_6$ and M_6C whereas the hardening is mainly imparted through the precipitation of fine semi-coherent M_2C particles.

The tempering behaviour of the two steels at the two different temperatures is found to differ in (i) the extent of secondary hardening, (ii) variation in the time to peak hardness and (iii) the saturation level of hardness at long tempering times. Generally, there is a rapid reduction in the hardness levels, though in certain combinations of temperature and prior microstructure, this stage is absent. The second feature, namely the secondary hardening, is observed in steel A at both the temperatures while only a very marginal secondary hardening is observed at 923K for steel B. The nature of hardening is more pronounced in steel A than in steel B. Further, the time to reach secondary hardening peak was higher at 923K than at 1023K in steel A. The saturation level of hardness at longer times at 923K for both the steels was higher than at 1023K.

Based on the above results, the tempering behaviour of the steel may be classified /15/ into four distinct stages, namely:

- Stage I representing initial softening
- Stage II representing the secondary hardening
- Stage III depicting the final softening
- Stage IV indicating the saturation.

During tempering, all the four stages were not present in both steels and at both the temperatures. Further, the stages were found to appear at different times at the two temperatures. Stage I was present in steel A for both the temperatures of interest, 923K and 1023K, while it is absent in steel B.

Stage II depicting the secondary hardening behaviour is present in steel A for both the temperatures of tempering. In contrast, steel B exhibits stage II only at 923K.

Stage III is found in both the steels and at both the temperatures of tempering but with significant difference in their final softening rates.

Stage IV, that is the saturation in hardness levels, is present in both the steels for both the tempering temperatures with different saturation levels.

The microstructural rationale for the occurrence of the different stages, the differences between the two different temperatures of tempering and prior microstructure discussed above, has been understood based on detailed TEM studies corresponding to the four stages. The details of these studies are discussed in the next section.

3.3.Microstructural basis for the tempering behaviour

Tempering at 1023K

Based on our present results summarised above, it is observed that when the steels are tempered at 1023K, stage I was found at much smaller times in Steel A compared to Steel B. Stage I, which is due to the modification of bainite into ferrite and carbides, takes place rapidly during the process of tempering in Steel A and hence was present for periods less than 2h in this steel.

The initial rapid softening was followed by stage II which becomes more dominant than stage I. This could be due to the appearance of fine needle-like precipitates of M_2C in the initial tempering period within 2h (Fig. 4 (a)) which are semi-coherent leading to secondary hardening. This clearly indicates that the kinetics favoured formation of M_2C at 1023K and the hardening due to M_2C more than offsets the softening caused by bainitic modification, thus resulting in the observed increase in hardness. However, the softening caused by the precipitation of other secondary carbides like M_7C_3, $M_{23}C_6$ and M_6C and the dissolution of M_2C resulted in the rapid softening at longer times of tempering. Fig. 4 (b) shows the carbon extraction replica of the steel A tempered for 20h. The micrograph depicts the presence of a number of carbides of different morphologies. Analysis of SAD patterns from different carbides showed that there is a coexistence of three different types of carbides, namely, M_7C_3, M_6C and $M_{23}C_6$. Typical SAD patterns and their analyses were shown in Fig. 4 (c,d), (e,f) and (g,h) indicating the zone axes as [0001] of M_7C_3, [150] of M_6C and [02$\bar{1}$] of $M_{23}C_6$ respectively.

In contrast, steel B showed a relatively simpler tempering behaviour. Steel B following its initial rapid softening simply goes over to stage III with a characteristic drop in the rate of softening and finally saturates into stage IV.

(a)

(b)

(c)

(e)

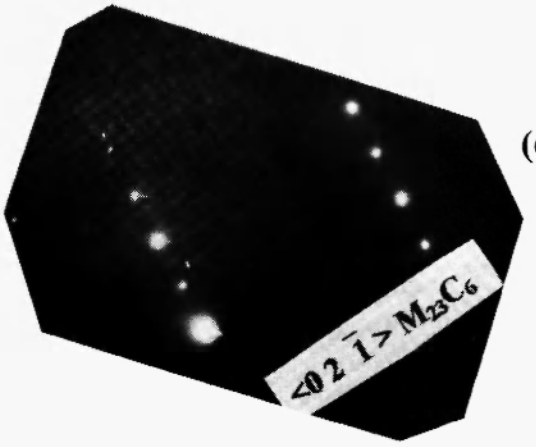

(d)

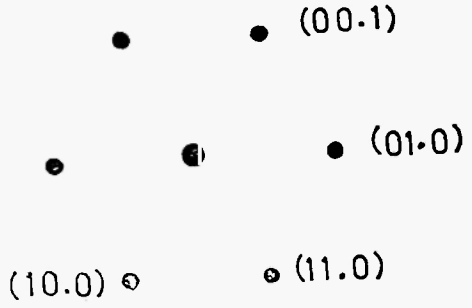

(f)

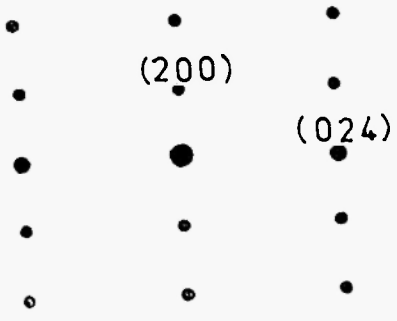

continued ...

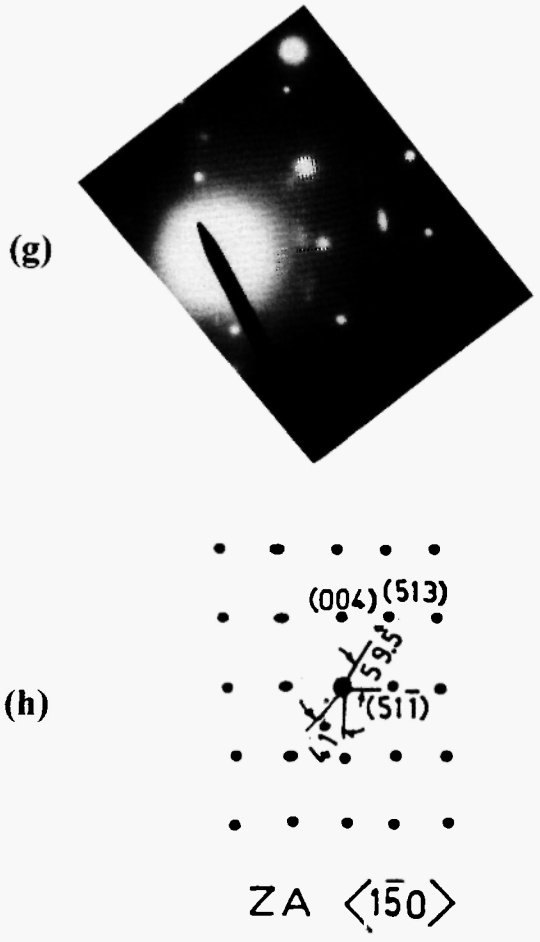

Fig. 4: Transmission electron micrographs showing the evolution of carbides in steel A tempered at 1023K:

(a) The fine needle-like M_2C carbides (arrow marked) in samples treated for 2h.

(b) Micrograph of the carbon replica microstructure of steel A treated at 1023K for 20h showing a variety of morphologies of carbides.

(c) SAD pattern of one of the carbides observed in Fig.4b showing the presence of M_7C_3 along [0001].

(d) Key showing the analysis of SAD pattern in (c)

(e) SAD pattern of one of the carbides observed in Fig.4b showing the evidence of $M_{23}C_6$.

(f) Key showing the zone axis is [0 2 $\bar{1}$] of $M_{23}C_6$.

(g) SAD pattern of one of the carbides observed in Fig.4b showing the evidence of M_6C.

(h) Key showing the zone axis is [1 $\bar{5}$ 0] of M_6C

Both steel A and steel B saturate around 160VHN. This could be due to the observation that the steels transform to completely defect-free ferrite and incoherent carbides like $M_{23}C_6$ and M_6C at longer tempering times. Further globularisation of carbides takes place, which also leads to softening of the matrix.

Fig. 5(a): Transmission Electron Micrograph depicting the globularisation of carbides and substructure formation in steel A when tempered at 1023K for 50h.

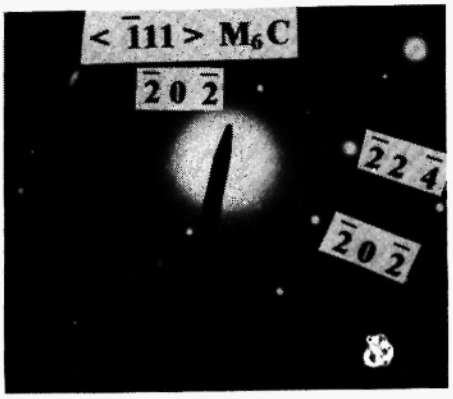

Fig. 5(b): SAD pattern of one of the carbides observed in Fig.5a showing the evidence of M_6C. The zone axis is [$\bar{1}$ 1 1].

Typical evidence for the coarsening observed in steel A is shown in Fig. 5(a). The analyses of these carbides were carried out using their SAD patterns [Fig. 5(b) and (c), (d)], which confirm the formation of M_6C and $M_{23}C_6$ respectively. These carbides are both FCC with nearly equal unit cell dimensions. However, it is known that M_6C is a Mo based carbide and $M_{23}C_6$ is a Cr based carbide. Hence their identification is carried out using EDX spectra. Typical spectra from the Cr-rich $M_{23}C_6$ and Mo-rich M_6C are presented in Fig. 5(e) and 5(f). The elemental distribution of Cr and Mo in the two carbides would continue to reach the equilibrium stoichiometry as the carbides continue to grow further on tempering till, the steel A and B reach equilibrium conditions with the formation of $Cr_{23}C_6$ and Mo_6C /14/.

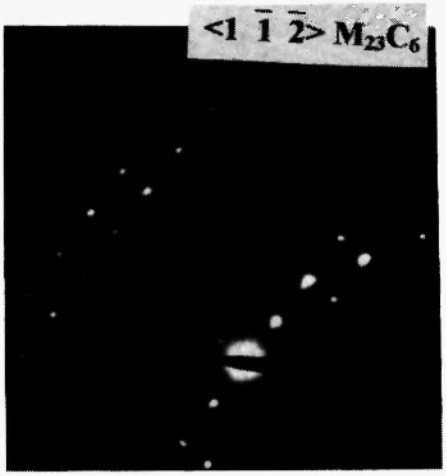

Fig. 5(c): SAD pattern of one of the carbides observed in Fig.5a showing the evidence of $M_{23}C_6$.

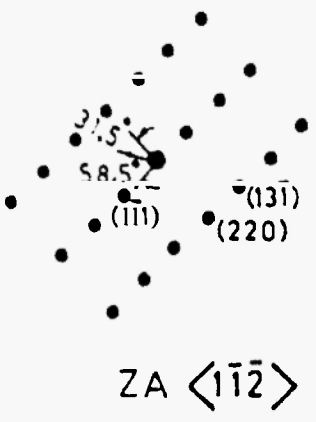

Fig. 5(d): Key shows the zone axis is [1 $\bar{1}$ 2].

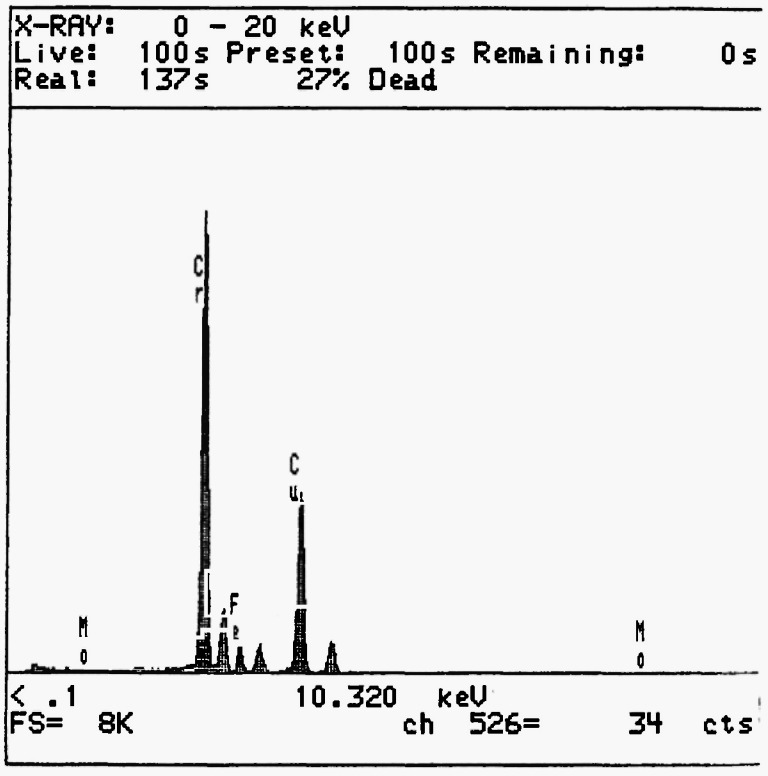

Fig. 5(e): EDX spectrum indicating the Cr-rich nature of $M_{23}C_6$. Cu peak is from the grid.

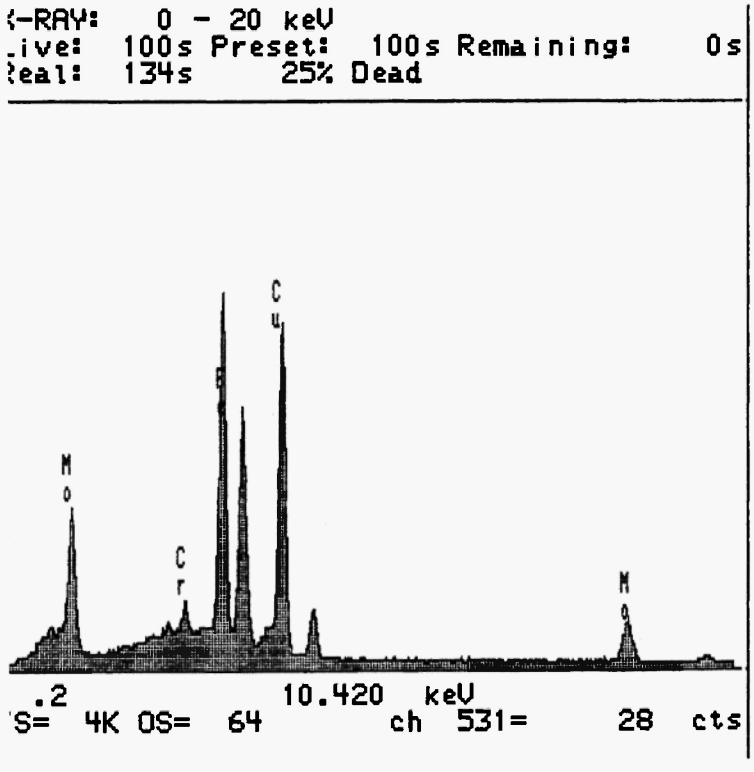

Fig. 5(f): EDX spectrum indicating the Mo-rich nature of M_6C. Cu peak is from the grid.

Tempering at 923K

When tempered at 923K, steel A showed a characteristic four-stage behaviour. Fig. 6 shows the typical optical micrograph of steel A tempered at 923K for 2h. It indicates that the tempering of the bainite has started. A detailed study using transmission electron

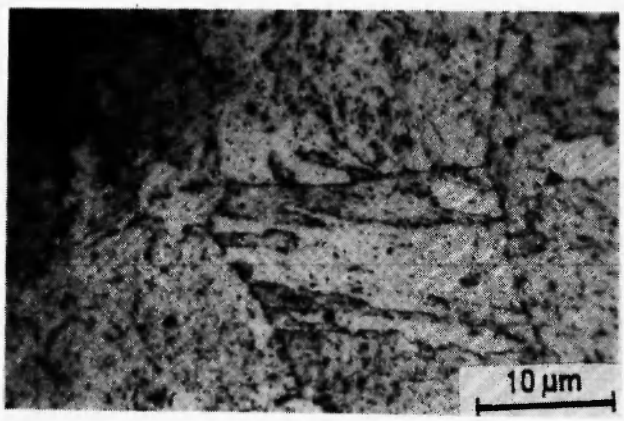

Fig. 6: Optical micrograph depicting the microstructure of steel A tempered at 923K for 2h.

microscopy revealed the presence of the lath structure of retained bainite and fine needles of M_2C (Fig. 7(a) and (b)). As the steel is tempered further for 10h, the modification of bainite was found to continue, as shown in Fig. 8a. This shows that the microstructure of the steel tempered for 10h, namely tempered bainite, has been modified to a lesser extent in comparison to tempering at 1023K (Fig. 4(b)). The sluggish rate of modification is due to slower kinetics prevalent at 923K in comparison to tempering at 1023K. A variety of secondary carbides were found to precipitate along with bainitic modification. Fig. 8(b) and (c) depict the typical modified bainite which retains the lath structure to a large extent with secondary carbides, which were identified by SAD patterns (see insets in Fig. 8(b) and (c)). The analyses show the zone axes of [0001] of M_7C_3 and [1 $\bar{1}$ 0] of $M_{23}C_6$.

The carbides were observed to precipitate along the lath boundaries of the retained bainite. The strengthening of the matrix by the copious precipitation of M_2C is also observed in steel A when it is tempered

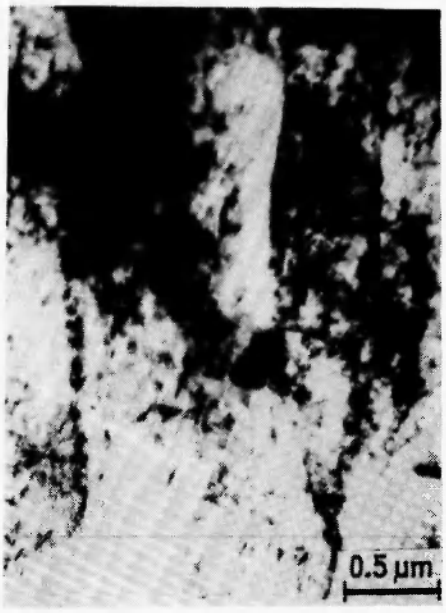

(a)

(b)

Fig. 7: Transmission electron micrographs of steel A tempered at 923K:
(a) The microstructure of steel A tempered for 2h. The bainitic laths are retained with fine needles of M_2C precipitation.
(b) The higher magnification picture of fig.7a showing the presence of fine needle-like M_2C in a cubic orientation.

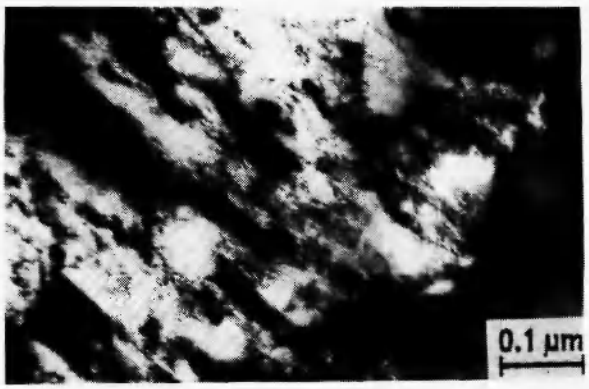

(a)

(b)

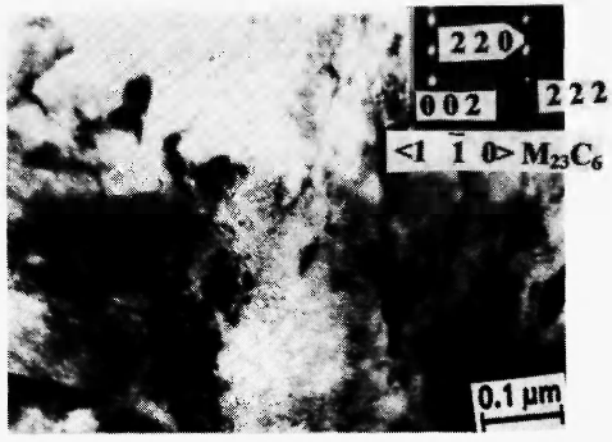

(c)

Fig. 8: Variation in microstructure of steel A tempered at 923K for 10h showing the
(a) retention of bainitic laths.
(b) presence of M_7C_3; the inset shows the zone axis as [0001]
(c) formation of coarse $M_{23}C_6$. The inset shows the SAD pattern of $M_{23}C_6$ along the zone axis [1 $\bar{1}$ 0].

for 20h at 923K. Fig. 9(a) confirms the evidence for the retention of needle-like semi-coherent precipitates of M_2C. On further tempering at 923K for over 50 hours, steel A exhibited recrystallisation and substructure formation (Fig. 9(b)) indicating complete modification of bainitic laths into subgrains of α-ferrite.

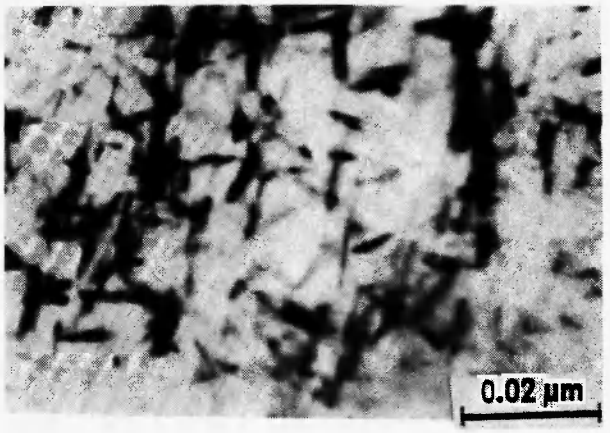

Fig. 9(a): Copious precipitation of M_2C that occurs in steel A tempered at 923K for 20h.

Fig. 9(b): The substructure development in steel A when treated at 923K for 50h.

On the other hand, steel B exhibited no initial softening feature typical of stage I. Instead a hardening peak indicating the effect of stage II is more dominant than the softening due to stage I. This is consistent with the presence of 70% ferrite in the steel. Fig. 10 shows that the steel B in the argon quenched condition itself exhibited bainite and ferrite. It shows, in addition, fine needles of M_2C, which on further tempering would

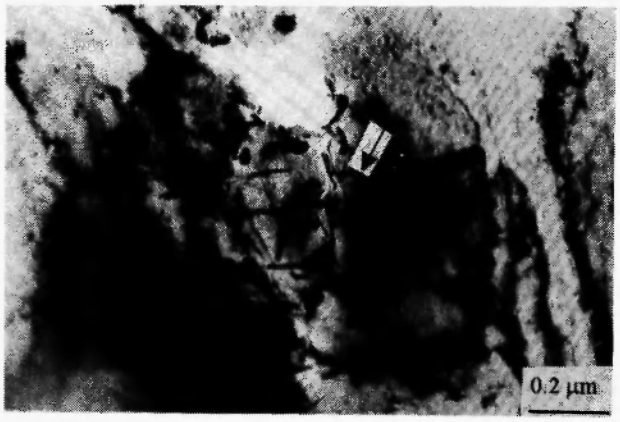

Fig. 10: Presence of needle-like M_2C precipitates in steel B in as-Argon quenched condition.

enable easy nucleation of additional M_2C carbides. On tempering for up to a period of 20h, it has resulted in evolution of M_7C_3 carbides. Fig. 11(a) shows the typical microstructure of steel B aged at 923K for 20h. The SAD pattern obtained from these carbides shown as inset in Fig. 11(a), clearly confirms the presence of

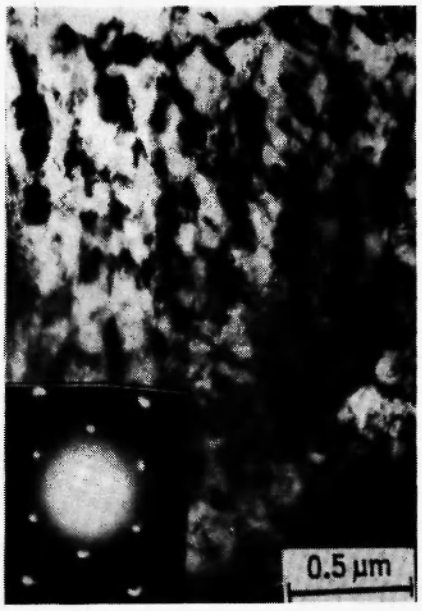

Fig. 11(a): Transmission electron micrograph of steel B tempered at 923K for 20h. The bainite is modified and precipitation of carbides observed. Inset shows the SAD pattern of one of the carbides indicating the presence of M_7C_3.

[0001] zone axis of M_7C_3 (key shown in Fig. 11.b). That is, the bainitic carbides (M_3C) have transformed into secondary carbides, which coarsened when tempered for 20h at 923K. On tempering for 50h, the modification of bainite into strain-free ferrite is complete though the M_2C carbides had not coarsened considerably (Fig. 11(c)). The retention of strengthening carbide, namely M_2C, for tempering times up to 50h has thus led to higher saturation level (Fig. 3) in contrast to the lower saturation level at a higher tempering temperature of 1023K.

Thus, during tempering, Steels A and B change in their initial microstructures and are in a continuous process of evolution towards equilibrium, where the carbides continue to coarsen /15/.

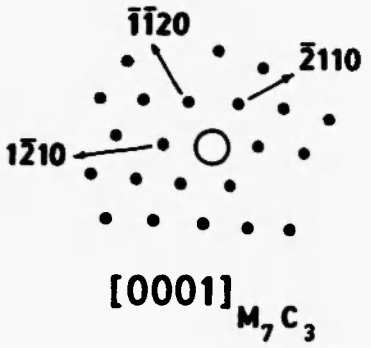

Fig. 11(b): shows the key for analysis of the SAD pattern shown in 11(a).

Fig. 11(c) Microstructure of steel B tempered for 50h. The ferrite-ferrite boundary shows the carbide precipitation. Ferrite region contains fine M_2C.

A schematic figure depicting the four stages and their corresponding microstructural rationale is shown in Fig. 12; stage I shows the start of tempering of the steel with the enhanced softening due to rapid modification of the metastable bainite into ferrite and carbides. This process manifests as changes in the lath structure of bainite, which becomes fully modified into dislocation-free ferrite grains with increasing time of exposure at the tempering temperatures.

Stage II was found to show a secondary hardening behaviour, which was rationalised, based on the precipitation of M_2C, which is found to be semi-coherent with the matrix. The coherency strains due to the formation of M_2C lead to an increase in hardness.

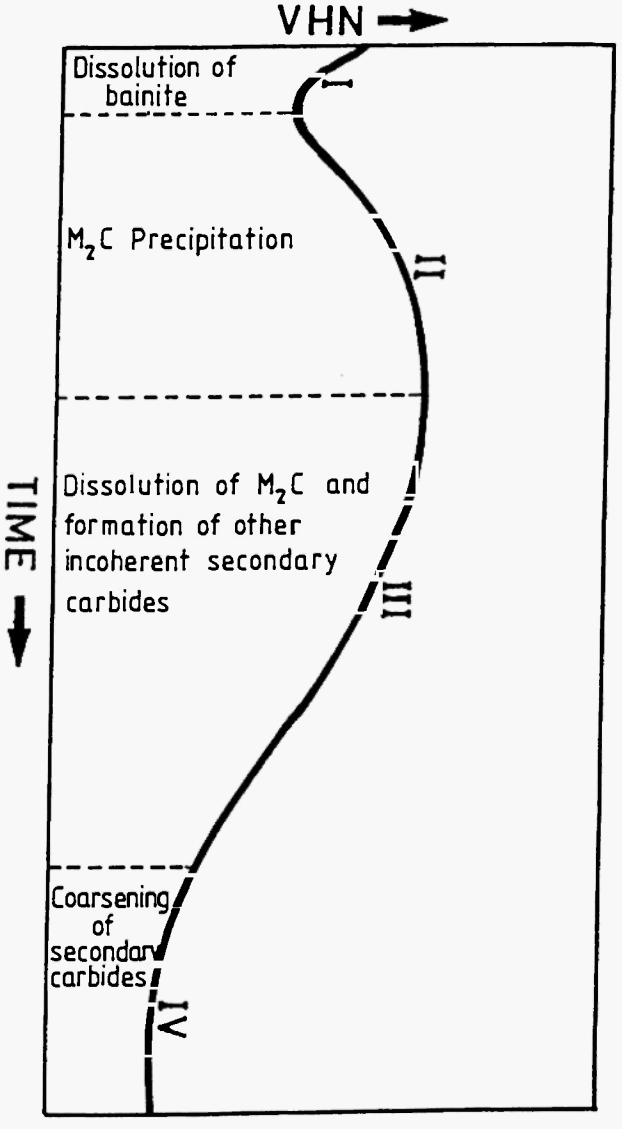

Fig.12: Schematic sketch showing the various stages of tempering along with their corresponding micromechanisms.

Stage III, which shows reduction in the hardness, is mainly contributed by the precipitation of other metastable carbides like M_7C_3, $M_{23}C_6$. These are incoherent in nature and hence soften the matrix to a larger extent.

Stage IV, depicting the saturation being achieved, is due to the balancing effects of the softening kinetics due to the secondary carbides and the hardening nature promoted by the M_2C precipitation. The saturation level depends on the volume fraction of M_2C that is retained. In case of complete dissolution of M_2C, the saturation level reaches the hardness of ferrite (140VHN) and is higher at lower tempering temperature due to retention of M_2C. The coarsening of all secondary carbides occurs during this stage.

Strengthening index (Σ)

In order to quantify the extent of the secondary hardening effect, a parameter called strengthening index is proposed. This can be expressed in terms of:

$$\text{Strengthening index, } \Sigma = \frac{\text{Maximum hardness - initial hardness}}{\text{Initial hardness}} \times 100$$

It is apparent from Fig.3 that the index is 10% for steel A and 2% for steel B at 923K respectively. It is observed from Fig. 3 that Steel A shows a similar strengthening index for 1023K also while steel B does not show any strengthening.

Let us consider the observation that the strengthening index at 923K is more in steel A than in steel B. This difference is due to the difference in the initial microstructures, which influences two factors: the degree of metastability and the nature of secondary carbides.

Steel A, exhibiting a complete bainitic structure that resulted from fast cooling, is more metastable than steel B due to its highly dislocated lath structure and higher concentration of carbon locked up in solution. It has been reported that the stored energy of a 100% bainitic steel is 780 J/mol more than the equilibrium state of the

steel, consisting of ferrite and carbides /16/. Therefore, the degree of metastability of steel A is expected to be much higher than in steel B.

It is known /12/ that bainite is relatively more suitable for the nucleation and growth of the semi-coherent M_2C carbides. However, in steel B, M_2C is expected to precipitate in the pro-eutectoid ferrite during cooling. This would be expected to be coarse and well distributed, thus not contributing significantly to the secondary hardening. On tempering, the M_2C would precipitate in the bainitic areas of steel B which are fine and semi-coherent. Although these carbides strengthen the steel B, the A_f of bainite is very low (30%) leading to a lower volume fraction of M_2C in steel B than in steel A at 923K.

In the case of steel A, no M_2C forms during cooling since cooling rate is faster. However, the bainitic regions of steel A favour formation of M_2C and these semi-coherent M_2C are finer and more dense than in steel B. This explains the high value of the strengthening index for steel A.

Usefulness of strengthening index

Thus a single parameter, namely the strengthening index, is useful in describing the influence of prior microstructure on the tempering behaviour. This parameter may be useful in assessing:

i) The in-service processing effects like repair welding on the subsequent microstructure. Presently efforts are in the direction of avoiding post-weld heat treatment procedures which would otherwise involve severe costs. This implies that the welded components would temper during service and the parameter can be used to assess the state of steel.

ii) Recent efforts to use thermomechanical forming to produce tubes have indicated that the microstructure is varied in nature /17/. Hence this index would be helpful in assessing the consequence of microstructural evolution in situations where a strip rolling by thermomechanical route is adopted.

4.CONCLUSIONS

- The tempering behaviour of 2.25Cr-1Mo steel at two temperatures, 923K and 1023K, for two different conditions of initial microstructures namely 100% bainite and (30% bainite+70% ferrite) is established. Based on hardness changes the tempering nature of the fully bainitic steel is found to be steep showing a larger extent of tempering in comparison to the ferrite-bainitic steel.
- The tempering behaviour has been classified into four stages: initial rapid softening (stage I), secondary hardening (stage II), final softening (stage III) and saturation (stage IV).
- The extent of the four stages of tempering behaviour was altered to a great extent by the prior microstructure.
- A parameter, namely strengthening index, is proposed for the quantification of the extent of secondary hardening.
- The strengthening index of Steel A is higher than that of Steel B due to a) higher degree of metastability of steel A as compared to steel B, b) higher number density of strengthening carbide like M_2C and c) uniform distribution of finer M_2C carbides in steel A than the coarse M_2C in steel B.

ACKNOWLEDGEMENTS

The authors wish to express their gratitude to Dr. Baldev Raj, Director, Materials, Chemistry and Reprocessing Group for his constant encouragement and keen interest in the study of ferritic steels.

REFERENCES

1. J. Orr, F.R. Beckitt and G.D. Fawkes, in: *Proc. Int. Conf. On Ferritic steels for Fast Reactor Steam Generators*, London, 1977, edited by S.F. Pugh and E.A. Little, (BNES., London,) 1978; p.91.
2. C.V. Sundaram, P. Rodriguez and S.L Mannan, *J. Min, Met.* (Inst. of Engineers, India), **67**, 1 (1986).
3. M.C. Murphy and G.D. Branch, *J.I.S.I.*, **546** (1971).
4. J.M. Titchmarsh, Harwell Report, AERE-R 9661 (1979).
5. R.L.Klueh, *J. Nuc. Mater.* **54**, 41(1974).

6. Wong Zhong-Gaung, K. Rahka, P. Nenonen and C. Laird, *Acta Metall* **33,** 2129 (1985).
7. F. Abe, H. Araki and T. Noda, *Mat. Sci. Technol.* **6,** 714 (1990).
8. John Piling and N. Ridley, *Met. Trans.* **13A,** 557 (1982).
9. R.Singh and S. Banerjee, *Mater.Sci. Engg.* **A132,** 203 (1990)
10. G.L. Dunlop and R.W.K. Honeycombe, *Met. Sci.* **10,**124 (1976).
11. P. Parameswaran, S. Saroja, M. Vijayalakshmi and V.S. Raghunathan, *J. Nuc. Mater.* **232,** 226 (1996).
12. R.G. Baker and J. Nutting, *J.I.S.I.* **192,** 257 (1959).
13. H.K.D.H. Bhadeshia, *Bainite in Steels* (The Inst. of Materials, London, UK., 1992; p. 107.
14. S. Saroja, P. Parameswaran, M. Vijayalakshmi and V.S. Raghunathan, *Acta.Mater.* **43**, 2985 (1995).
15. P. Parameswaran, M. Vijayalakshmi, P. Shankar and V.S. Raghunathan, *J. Mater. Sci.* **27**, 5426 (1992).
16. H.K.D.K. Bhadeshia, A. Strang and D.J. Gooch, *Int. Mater. Rev.* **3,** 45 (1998).
17. Roh TaeHoon, Private communication.